

1 **Development of a dynamic dust-source map for NMME-DREAM v1.0 model based on MODIS**  
2 **NDVI over the Arabian Peninsula**

3 Solomos Stavros<sup>1,2</sup>, Abdelgadir Abuelgasim<sup>2\*</sup>, Christos Spyrou<sup>3</sup>, Ioannis Biniotoglou<sup>4</sup>, Slobodan  
4 Nickovic<sup>5</sup>

5 **Abstract** We developed a time dependent dust source map for NMME-DREAM v1.0 model  
6 based on the satellite MODIS Normalized Difference Vegetation Index (NDVI). Areas with  
7 NDVI<0.1 are classified as active dust sources. The updated modeling system is tested for dust  
8 emission capabilities over SW Asia using a mesoscale model grid increment of 0.1°×0.1° km for  
9 a period of one year (2016). Our results indicate significant deviations in simulated Aerosol  
10 Optical Depths compared to the static dust-source approach and general increase in dustloads  
11 over the selected domain. Comparison with MODIS Aerosol Optical Depth (AOD) indicates a  
12 more realistic spatial distribution of dust in the dynamic source simulations compared to the  
13 static dust sources approach. The modeled AOD bias is improved from -0.140 to 0.083 for the  
14 case of dust events (i.e. for AOD >0.25) and from -0.933 to -0.424 for dust episodes with  
15 AOD>1. This new development can be easily applied to other time periods, models and  
16 different areas worldwide for a local fine tuning of the parameterization and assessment of its  
17 performance.

18 <sup>1</sup> Institute for Astronomy, Astrophysics, Space Applications and Remote Sensing (IAASARS), National Observatory of Athens,  
19 Athens, Greece, stavros@noa.gr

20 <sup>2</sup> Department of Geography and Urban Planning, National Space Science and Technology Center, United Arab Emirates  
21 University

22 <sup>3</sup> Department of Geography, Harokopio University of Athens (HUA), El. Venizelou Str. 70, 17671 Athens, Greece.

23 <sup>4</sup> National Institute of R & D for Optoelectronics, Magurele, Ilfov, Romania

24 <sup>5</sup> Republic Hydrometeorological Service of Serbia, Belgrade, Serbia

25 \*Corresponding author

26 **Keywords:** dust, Arabian Peninsula, DREAM, NDVI, model, satellite

27 **Introduction**

28 The importance of natural particles, namely desert dust, in the weather and climate has  
29 been underlined in a great number of studies. Dust is a climatic regulator, as it modifies  
30 extensively the radiative balance of the atmospheric column (e.g. Torge et al., 2011; Spyrou et  
31 al., 2013; Mahowald et al., 2014). At the same time dust aerosols modify the atmospheric water  
32 content (Spyrou 2018), the way clouds are formed by acting as cloud condensation nuclei (CCN)  
33 and ice nuclei (IN) and the precipitation process (Kumar et al., 2011; Solomos et al., 2011;  
34 Nickovic et al., 2016). In addition, there is a clear connection between dust particles and human  
35 health disorders, as the size of the produced aerosols is small enough to cause respiratory and  
36 cardiovascular diseases, as well as pathogenic conditions due to the microorganisms that they  
37 can potentially carry (Mitsakou et al., 2008; Esmail et al., 2014).

38 The Arabian Peninsula is one of the most important sources of mineral dust worldwide and  
39 contributes together with the Saharan and Gobi Deserts in the formation of a North  
40 Hemisphere “dust belt” as described by Prospero et al. (2002). Severe dust storms over the  
41 Peninsula are quite common, especially during long periods without rain, in the spring and  
42 summer (Almazrouia et al., 2012). Particles injected into the atmosphere from arid soils, under  
43 favorable weather conditions (high wind speeds and dry soil), can affect large areas around the  
44 sources but also remote locations like the Eastern Mediterranean (Mamouri et al., 2016;  
45 Solomos et al., 2017) and the Indian Ocean (Chakraborty et al. 2006).

46 Due to the multitude and severe effects of dust particles not only on the weather and the  
47 ecosystem but to human health as well, the proper description of the production, transport and  
48 eventual deposition of the dust cycle, in numerical weather prediction models (NWP) is  
49 essential. In order to be able to accurately describe the dust life-cycle in the atmosphere, we  
50 need a clear understanding of the areas which can potentially act as “dust sources”. The  
51 definition of such areas dictates the emission strength and therefore the amount of particles  
52 inserted into the atmosphere. A proper representation of dust sources is therefore an essential  
53 first step, in studying the impacts of mineral particles in the climate and human societies.  
54 Usually the definition of the areas that can act as dust sources is made using global datasets.  
55 For example Nickovic et al. (2001) used a subjective correspondence between the Olson World  
56 Ecosystems (Olson et al., 1983) and the thirteen SSib (simplified simple biosphere, Xue et al.  
57 1991) vegetation types to identify arid and semi-arid areas. Similarly, Spyrou et al., (2010) used  
58 a 30sec global land use/cover database, classified according to the 24 category U.S. Geological  
59 Survey (USGS) land use/cover system (Anderson et al., 1976), to define active areas in SKIRON  
60 dust model. Solomos et al., (2011) used the LEAF soil and vegetation sub-model of the Regional  
61 Atmospheric Modeling System (RAMS) (Walko et al., 2000) to identify the active dust sources in  
62 RAMS-ICLAMS model.

63 However, the above-mentioned methodologies have some significant drawbacks. The  
64 datasets are usually not up-to-date, therefore recent land-use modifications are not included  
65 and not represented. In addition, such “static” databases mean that possible seasonal  
66 variations are not taken into account. Towards the direction of overcoming the above  
67 limitations and improving global dust forecasts, Kim et al., (2013) developed a dynamical dust  
68 source map for the GOCART dust model by characterizing NDVI values  $< 0.15$  as active dust  
69 spots. Similarly Vukovic et al., (2014) combined MODIS landcover types with pixels having NDVI  
70  $< 0.1$  to identify the seasonal dust sources that enforced the severe Phoenix haboob of July  
71 2011 in the US. Such information can be even more relevant at meso and local scales for  
72 determining landuse changes and potential dust sources, especially in heterogeneous regions  
73 such as the Arabian Peninsula (which has more diverse soil types than e.g. the Sahara Desert)  
74 and the greater SW Asia. In this context, Solomos et al., (2017), used the Landsat-8 NDVI data  
75 (assuming also NDVI $<0.1$  as active sources) to identify recent changes in landuse due to the war  
76 in Iraq and Syria resulting in a significantly more realistic simulation of dust properties in the  
77 Middle East.

78 In the current study we present the implementation of a dynamical dust source map in the  
79 well-established and widely used DREAM v1.0 dust model (Nickovic et al., 2001; Perez et al.,  
80 2006). The new development is first tested here for the greater SW Asia but can be extended  
81 for use in mesoscale dust modeling applications worldwide. Two experimental simulations are

82 performed for one month period (August 2016) over the greater SW Asia: 1) Control run, where  
 83 the dust source definition is based on the Ginoux et al., (2001) dataset and 2) Dynamic source  
 84 run, where the NDVI values are used to identify the dust sources. The main differences in our  
 85 approach compared to the previous studies referenced above, is that we use a very high  
 86 resolution NDVI product (500x500 m) in a regional modeling domain (e.g. Kim et al., 2013 used  
 87 an 8x8 Km NDVI dataset extrapolated to 1°x1° global modeling domain) and our study is not  
 88 limited to specific test cases (like for example Vukovic et al., 2014 and Solomos et al., 2017),  
 89 but covers an extended time period, as presented below. The model results from both runs are  
 90 compared to available satellite observations and station measurements inside the modeling  
 91 domain. In section 1 we describe the methodological steps regarding the model developments  
 92 and remote sensing data; Section 2 includes the results of the experimental runs and section 3  
 93 is a summary and discussion of the study findings.

94  
 95

## 96 **1. Methodology**

97

### 98 **1.1. Model description**

99 The modeling system used in this study is NMME-DREAM v1.0. The meteorological core is  
 100 the NCEP/NMME atmospheric model (Janjic et al., 2001). The Dust Regional Atmospheric Model  
 101 (DREAM v1.0) is a numerical model created with the main purpose to simulate and predict the  
 102 atmospheric life-cycle of mineral dust using an Euler-type nonlinear partial differential equation  
 103 for dust mass continuity (Nickovic et al., 2001; Perez et al., 2006; Pejanovic et al., 2011, Nickovic  
 104 et al., 2016). In DREAM the concentration approach is used for dust uplift, where surface  
 105 concentration is used as a lower boundary condition and used for the calculation of surface  
 106 fluxes, which in turn depends of the friction velocity (Nickovic et al., 2001). This surface  
 107 concentration is calculated using equation (11) from Nickovic et al., (2001):

108

$$109 \quad C_{sfc} = c_1 \cdot \delta \cdot u_*^2 \left[ 1 - \left( \frac{u_{*t}}{u_*} \right)^2 \right] \quad \text{where } c_1 = 2.4 \cdot 10^{-4} \frac{Kgr}{m^5 \text{ sec}^2} \text{ a constant determined from model}$$

110 experiments,  $u_*$  and  $u_{*t}$  the friction velocity and the threshold friction velocity for dust  
 111 production respectively and  $\delta = a \cdot \gamma_k \cdot \beta_k$ , where  $\gamma_k$  the ratio between the mass available for  
 112 uplift and the total mass  $\beta_k$  the fractions of clay, silt and sand for each soil class, and  $a$  the  
 113 desert mask (between 0 and 1) calculated from the Ginoux et al., (2001) dataset. Soil moisture  
 114 and particle size dictate the threshold friction velocity which initializes dust production. Once  
 115 particles have been lifted from the ground they are driven by the atmospheric model variables  
 116 and processes. Therefore turbulent parameters are used in the beginning of the process, when  
 117 dust is lifted from the ground, and transported by model winds in the later phases when dust  
 118 travels away from the sources. The model handles dust in eight size bins, with effective radii of  
 119 0.15, 0.25, 0.45, 0.78, 1.3, 2.2, 3.8, and 7.1 mm. Dust is treated as a passive tracer and doesn't  
 120 interact with radiation or clouds. Dust is eventually settled through rainfall and/or dry  
 121 deposition processes parameterized according to the scheme of Georgi (1986) which includes

122 deposition by surface turbulent and Brownian diffusion, gravitational settling and impact on  
123 surface elements.

124 In order to test the use of NDVI for source characterization, the model is setup with a horizontal  
125 resolution of 0.1°x0.1°, covering the Arabian Peninsula parts of SW Asia and parts of NE Africa  
126 (Figure 1). On the vertical we use 28 levels stretching from the surface to the top of the  
127 atmosphere. August 2016 has been selected as a test period for the model development due to  
128 the significant dust activity and variability in wind properties during this month. One-year runs  
129 for the entire 2016 have been conducted to evaluate the performance of the static and  
130 dynamic database emission maps. The original classification of dust sources in DREAM is based  
131 on Ginoux et al., (2001) that takes into account the preferential sources related to topographic  
132 depressions and paleolake sediments. The global mapping of dust sources in Ginoux et  
133 al.,(2001) is determined from the comparison between the elevation of surface grid points at  
134 1°x1° resolution with the surrounding hydrological basins and with the 1°x1° AVHRR (Advanced  
135 Very High Resolution Radiometer) vegetation map (DeFries and Townshend, 1994). Recent  
136 studies indicated the contribution of both natural and anthropogenic dust sources to the overall  
137 dust emissions detected in MODIS Deep Blue product (Ginoux et al., 2012) and also the  
138 relevance of local geomorphological conditions and sediment supply (Parajuli and Zender,  
139 2017) on the global dust emissions. All these advances in dust emissions are based on static  
140 map considerations.

141 In our work, a numerical procedure has been developed to insert the NDVI satellite information  
142 into the model and to update such info each time the NDVI changes, during the simulation  
143 period. We assume that regions with NDVI values from 0 to 0.1 correspond to bare soil and  
144 therefore can be efficient sources (“dust points”; DeFries and Townshend, 1994; Solomos et al.,  
145 2017). In general it is not easy to define a global threshold value for all satellite NDVI sensors  
146 and all vegetation types worldwide. For example Kim et al. (2013) used a threshold of 0.15 to  
147 define global dust sources based on AVHRR retrievals (Tucker et al., 2005; Brown et al., 2006).  
148 Here we adopt the 0.1 NDVI threshold due to the bareness of the specific modeling domain  
149 since a higher value could overestimate the regional dust sources. The NDVI dataset is at finer  
150 resolution than the model grid (500x500 m) and in order to find the potential for dust  
151 production in each model grid box, we calculate the following ratio:

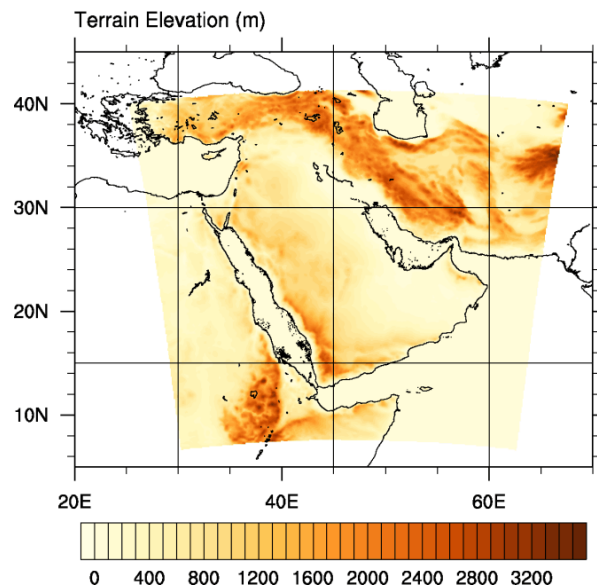
$$A_{grid\_box} = \frac{\#\_of\_dust\_points}{Total\_#\_of\_points}$$

152  
153 Where  $\#\_of\_dust\_points$  is the number of points with NDVI values smaller than 0.1. This  
154 approach allows for a dynamic description of dust source areas over the model domain to  
155 replace the previously used static database. Moreover, the scaling of satellite data over model  
156 grid points allows the use of the same algorithm for different model configurations. Several  
157 mountains in the area (e.g. the Sarawat Mountains along the Red Sea coast and the Zagros  
158 Mountains in Iraq) could be misclassified as dust sources due to low NDVI values. In order to  
159 exclude such unrealistic emissions from non-soil bare areas or snow-covered areas we have  
160 applied a limit of zero dust production above 2500 m over the entire domain. This simple  
161 approach has been selected in order to keep our straightforward NDVI mapping independent of  
162 vegetation and soil information. The threshold value of 2500 m does not suppress the

163 emissions from lowlands and hillsides (e.g. the coastal areas of Hejaz Mountains in Red Sea that  
164 have been identified as hot dust spots by Anisimov et al., 2017).

165 In Figure 2a we show the static sources in the original model version with a factor of 0 to 1  
166 depending on the source area strength. Accordingly in Figure 2b we show the new dynamic  
167 sources for 1-16 of August 2016. The two dust source patterns present remarkable difference  
168 especially over the western Saudi Arabia and over Iran and Pakistan where the NDVI  
169 classification results in stronger emissions. In order to test the performance of the new  
170 methodology we run the model in two different configurations: (1) Using the static Ginoux et  
171 al., (2001) dust source database, called DREAM-CTRL run from now on, and (2) using the  
172 dynamic NDVI database as described above, called DREAM-NDVI run from now on. Both setups  
173 are initialized using the NCEP GFS analysis files (0.5°×0.5° at 00, 06, 12 and 18 UTC), which were  
174 used for boundary conditions as well. The two model configurations are identical other than the  
175 dust source database.

176



177

178

**Figure 1: DREAM model domain and topography in meters**

179

## 1.2 NDVI description

180

181

182

183

184

185

186

187

188

189

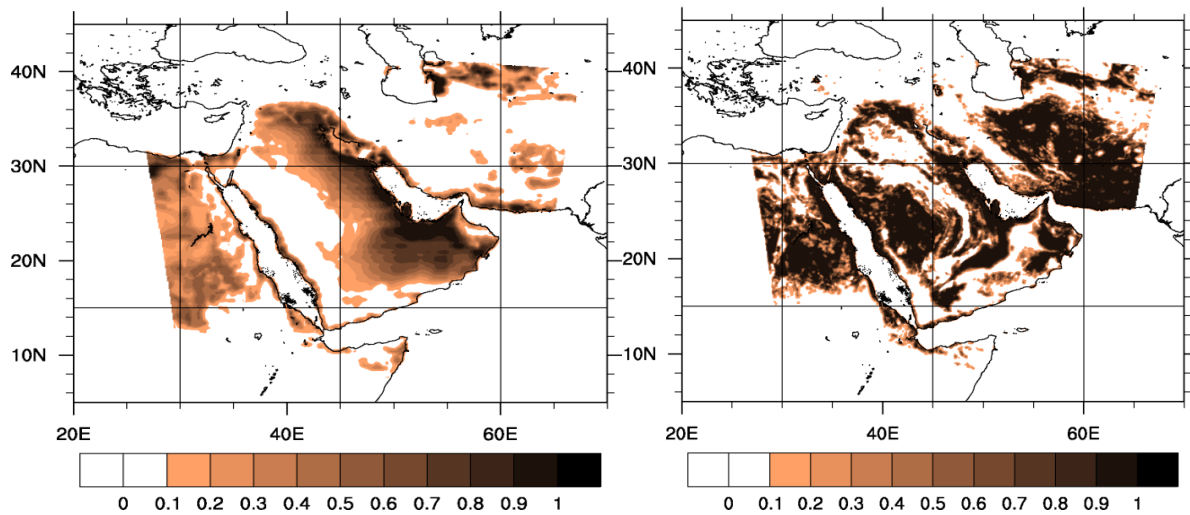
For the purposes of our study we used the 500m 16-day averaged NDVI from MODIS (Didan, 2015) for the period of interest. The NDVI is a normalized transform of the near infrared to red reflectance ratio, designed to provide a standard for vegetation and takes values between -1 and +1. Since it is expressed as a ratio, the NDVI has the advantage of minimizing certain types of band-correlated noise (positively-correlated) and influences attributed to variations in irradiance, clouds, atmospheric attenuation and other parameters (Solano et al., 2010).

To create an accurate time-dependent dust source map, we have utilized the Normalized Difference Vegetation Index (NDVI) derived from the MODIS/Terra instrument. NDVI is calculated as the normalized difference of reflectance in the red and near-infrared channels (Rouse et al., 1974; Huete et al. 2002) i.e.,

190

$$NDVI = \frac{X_{nir} - X_{red}}{X_{nir} + X_{red}}$$

191 where X represents surface reflectance as would be measured at ground level (i.e. corrected for  
 192 atmospheric gas and aerosol effects).in each channel. The 16-day composite is calculated by  
 193 ingesting two 8-day composite surface reflectance granules, taking into account pixel quality,  
 194 presence of clouds, and viewing geometry. This procedure can lead to spatial discontinuities, as  
 195 it is possible that data from different days are used for adjacent pixels, each representing  
 196 different measurement conditions. If a pixel had no useful measurements during the 16-day  
 197 period, historic data are used as fill values (Didan et al., 2015). For terrestrial targets, NDVI will  
 198 take values near 0.8 for vegetated areas and near 0 for barren soil (Huete et al., 1999). The  
 199 high-resolution dataset was used to calculate the percentage of barren land in each 0.1°x0.1°  
 200 model grid cells and this percentage was used to define the effective strength of dust sources in  
 201 each cell.  
 202



203  
 204  
 205  
 206

**Figure 2: Dust source strength as defined by (a) the Ginoux et al., 2001 dataset and (b) the 16th of August 2016 mean NDVI**

207 **1.3 Evaluation datasets and metrics**

208 Model evaluation is carried out two datasets. First, the MODIS monthly aerosol optical depth  
 209 (AOD) is use to study the spatial distribution of dust in the model domain. For this we use the  
 210 level 3 gridded atmosphere monthly product at 1x1 resolution, MOD08\_ME (Platnick et al.  
 211 2017). Secondly, we evaluate model performance using AERONET AOD retrievals at 8  
 212 photometric stations. AERONET is a network of sun/sky photometers that derive aerosol  
 213 optical and microphysical properties at a large number of stations around the world (Holben et  
 214 al., 1998). For this evaluation, we use Version 3 AOD retrievals that, in comparison with  
 215 previous versions, improves automatic cloud screening (Giles et al, 2018). Level 2 datasets were  
 216 used for all stations apart from Kuwait University, where only Level 1.5 data were available.  
 217 Both model and AERONET AOD were calculated at 532nm; this was chosen to facilitate future  
 218 intercomparing against lidar systems that frequently measure at this wavelength (e.g.  
 219 Pappalardo et al., 2014). AERONET measurements were converted to this wavelength using the

220 440-870 angstrom exponent and taking into account AOD measurements at 440nm, 675nm,  
221 and 870nm; in the cases where the 440nm AOD was not available, the 500nm (Mezaira) or  
222 443nm (KAUST campus) measurement was used instead.

223

224 We evaluate model performance using five metrics: mean bias, root mean square error,  
225 correlation coefficient, mean fractional bias, and fractional gross error. Concretely, assuming  
226 we have n pairs of model values ( $m_i$ ) and observations ( $o_i$ ), the mean bias (MB) is defined as:

$$227 MB = \overline{m_i - o_i}$$

228 where the bar denotes the mean value. Root mean square error (RMSE) is defined as

$$229 RMSE = \sqrt{\overline{(m_i - o_i)^2}}$$

230 The correlation coefficient (r) is defined as

$$231 r = \frac{\sum_{i=1}^n (m_i - \bar{m})(o_i - \bar{o})}{\sqrt{\sum_{i=1}^n (m_i - \bar{m})^2} \sqrt{\sum_{i=1}^n (o_i - \bar{o})^2}}$$

232 The fractional gross error (FGE) is defined as

$$233 FGE = 2 \frac{|m_i - o_i|}{m_i + o_i}$$

234 following Boylan and Russell, 2006. Similarly, mean fractional bias (MFB) is defined as

$$235 MFB = 2 \frac{\overline{m_i - o_i}}{\overline{m_i + o_i}}$$

236

237

238 following Chang and Hanna, 2004.

239

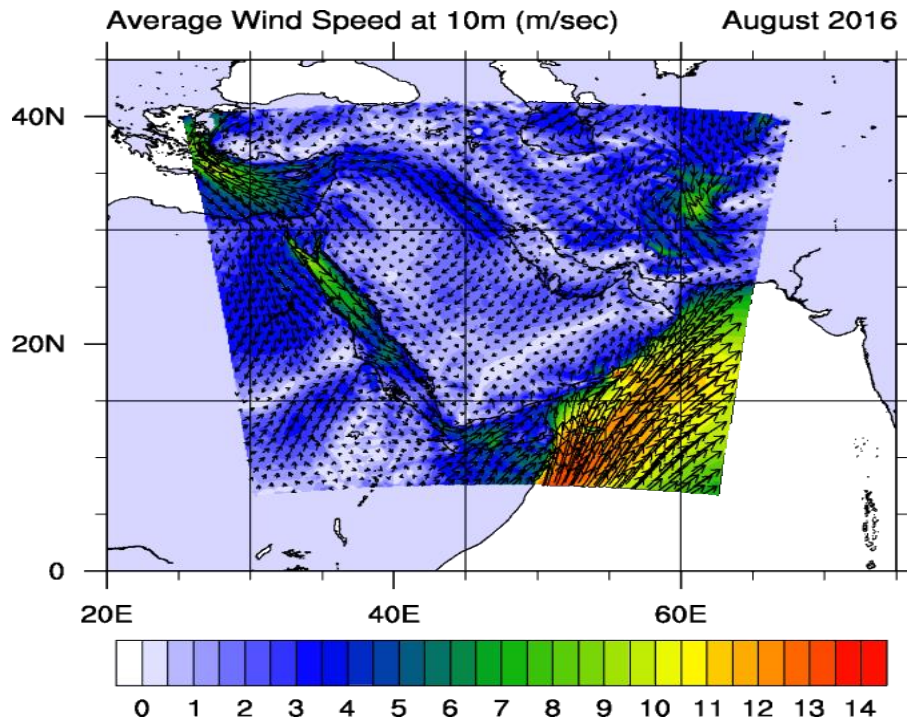
240

## 241 **2. Results**

242 DREAM-CTRL runDREAM-NDVI runThe test simulation period is 1-31 August 2016 and the  
243 results from both simulations are compared to MODIS and AERONET AOD. A five days spin up  
244 model run, prior to the experimental period, is used for establishing the dust background over  
245 the domain. After finalizing the experimental model configuration we perform a complete one-  
246 year run (2016) and evaluate the results against AERONET stations.

### 247 **2.1 Dust transport during August 2016**

248 The selected 1-month period is characterized by a significant variability in wind speeds and  
249 directions (Figure 3) which allows the evaluation of the new model version under different  
250 conditions. During 1-10 August, east winds prevail over the region and increased dust  
251 concentrations are found mostly along the central, east and south coastal areas of the Arabian  
252 Peninsula. An anticyclonic circulation is established during 10-15 over the Arabia Desert and  
253 increased dust concentrations are mostly found over the central desert areas. On 16-26 August  
254 the circulation is mainly from north directions and thick dust plumes are advected southwards  
255 towards the Arabian Sea. The north winds veer to east on 26-31 August and increased  
256 dustloads are found over the Gulf during these dates.



257

258 Figure 3. Average wind speed (color scale) and vectors from NMME-DREAMv1.0 for August  
259 2016.

## 260 2.2 Comparison with MODIS and AERONET

261 The monthly average AOD for August 2016 is shown in Figure 4 for the two experimental runs  
262 (Figure 4a, b). The DREAM-NDVI run results in a significantly modified spatial distribution of  
263 dust presenting increased dustloads over the entire domain and most profoundly over the Red  
264 Sea and Gulf regions (Figure 4b). This dust pattern is closer to the MODIS observed AOD over  
265 the same period that is shown in Figure 4c. The MODIS AOD in this area is mostly related to  
266 dust, however it must be taken into account that other aerosols not parameterized in the  
267 model (e.g. sea salt, sulphates, nitrates) may also contribute to the observed MODIS AOD.

268 The first step is to examine how our methodology compares against the monthly average AOD  
269 in our study area. Therefore the monthly average AOD values produced from our two  
270 simulations (DREAM-NDVI run and DREAM-CTRL run) are compared. More specifically the  
271 DREAM-NDVI run reproduces the MODIS observed AOD pattern that is in general characterized  
272 by values 0.3-0.4 at the NW parts of the Arabian Peninsula and by values 0.4-0.8 at the SE parts.  
273 Significant improvement is also evident over the Red Sea and NE Africa. The DREAM-NDVI run  
274 captures the maximum observed AOD values reaching up to 1.6 over the Red Sea and also the  
275 southwesterly extension of an AOD tongue of 0.3-0.8 towards Soudan. At the east parts of the  
276 modeling domain the DREAM-NDVI run again outperforms the DREAM-CTRL run since it  
277 reproduces the spatial distribution of AOD 0.4-0.8 over the Arabian Sea and the maximum of  
278 0.8-1.2 at the SE edge of Arabian Peninsula. Inside the Gulf, the NDVI run correctly represents  
279 the 0.4-0.8 AOD but the dust concentration is over-predicted at the Strait of Hormuz and along  
280 the Iran - Pakistan coastline. This is mostly due to the prevailing NE winds during the last days of



281 the August 2016 modeling period and due to a possible miss-classification of Iran and Pakistan  
282 grid points as effective dust sources thus favoring unrealistic southeasterly transport towards  
283 the Gulf of Oman. The DREAM-NDVI AOD is also higher than MODIS AOD over western Saudi  
284 Arabia indicating a possible overprediction of dust sources at this area.

285 As a second step we run the same model configurations (CTRL and NDVI) for the entire 2016.  
286 The modeled dust optical depth is compared with individual AERONET measurements. The  
287 model retrievals are interpolated in time to match the AERONET measurement time  
288 considering only dust relevant measurements with Angström Coefficient  $<0.6$  (Holben et al.,  
289 1998) and the results are shown in Table 1. For completeness we first consider all AERONET  
290 stations inside the modeling domain for the evaluation. However the stations that are at the  
291 margins of our domain (Cairo\_EMA\_2, SEDE\_BOKER, AgiaMarina\_Xyliatou and El\_Farafra) are  
292 also affected by other dust source areas (e.g. Sahara Desert) and their statistics are not  
293 representative for Arabian and Middle East sources. Instead, the comparison with Arabian  
294 Peninsula stations (Eilat, Kuwait\_University, KAUST\_Campus and Mezaira) provides more  
295 insight on the effects of the new source characterization. As seen in Figure 5 and also in Table 2  
296 these stations are clearly benefited from the experimental run.

297 In general the two runs present a significant statistical difference and more remarkably a  
298 reverse of bias (MODEL-AERONET) from negative in the DREAM-CTRL run to positive in the  
299 DREAM-NDVI run. The DREAM-NDVI run produces increased AODs that are neither linearly  
300 proportional to the DREAM-CTRL run AODs nor uniformly distributed over the domain. When  
301 considering only Arabian stations, the statistical metrics in Table 1 and especially the fractional  
302 gross error and bias are improved but the RMSE is increased due to the increase in maximum  
303 modeled AODs. In order to investigate the sensitivity of our results towards the severity of dust  
304 events we further assume two additional air quality states in Table 1: (i) dust events ( $AOD > 0.25$ )  
305 and (ii) severe dust episodes ( $AOD > 1$ ). Both cases show an improvement in the bias values over  
306 the control simulations. When we consider  $AOD > 1$  the DREAM-NDVI run still underestimates  
307 the observed values, but with a lower RMSE (0.586 versus 0.983 of the DREAM-CTRL run). This is  
308 clearly evident in Figure 6 where the NDVI run is indeed more realistic for the Arabian stations  
309 but still does not reproduce the extreme AOD during severe episodes. For most of the cases  
310 such high AODs should be attributed to duststorms from convective downdrafts (haboobs).  
311 These processes are not resolved at mesoscale model resolutions (Solomos et al., 2012, 2017;  
312 Vukovic et al., 2014) and thus cannot be represented here.

313 **Table 1. Statistical metrics from the comparison between the annual runs and AERONET**

	Mean bias (Model-Observation)		RMSE		Correlation		Fractional gross error		Mean fractional bias	
	CTRL	NDVI	CTRL	NDVI	CTRL	NDVI	CTRL	NDVI	CTRL	NDVI
AOD > 0 (All Stations)	-0.163	0.015	0.258	0.312	0.408	0.464	0.887	0.803	-0.639	0.043
AOD > 0 (Arabia Stations)	-0.142	0.122	0.252	0.332	0.340	0.426	0.644	0.515	-0.455	-0.187
AOD > 0.25 ( Arabia Stations )	-0.140	0.083	0.283	0.350	0.238	0.328	0.640	0.462	-0.527	-0.142
AOD > 1 ( Arabia Stations )	-0.933	-0.424	0.983	0.586	0.032	0.009	1.230	0.481	-1.211	-0.413

The AERONET stations used in this study are: Eilat (29N,34E), Cairo\_EMA\_2 (30N,31E), Kuwait\_University (29N,47E), KAUST\_Campus (22N,39E), SEDE\_BOKER (30N,34E), AgiaMarina\_Xyliatou (35N,33E), Mezaira (23N,53E) and El\_Farafra (27N,27E)

314

315 **3. Summary and Discussion**

316 In this study we present the development of a dynamic dust source map for implementation in  
 317 NMME-DREAM v1.0 over the Arabian Peninsula and the greater areas of Middle East, SW Asia  
 318 and NE Africa. Although the major dust sources worldwide are located in permanent deserts  
 319 where the NDVI is almost always <0.1 (e.g. Bodele Depression, Gobi Desert, Arabian Desert),  
 320 the dynamical scaling of dust emissions presented here can be important for providing up-to-  
 321 date evidence of active dust sources over non-permanent deserts. These may include dried  
 322 bog, marshes and semi-desert areas as well as irrigated and non-irrigated farms where landuse  
 323 changes occur throughout the year. Analysis of the modeling results for one year test period  
 324 (2016) over SW Asia indicated the improved performance of the new parameterization. The  
 325 DREAM-NDVI run showed a significant increase in dustloads over the greater Arabian Peninsula  
 326 area and a more realistic representation of the spatial distribution of AOD compared to the  
 327 corresponding MODIS satellite retrievals. These findings support the previous results by Kim et  
 328 al., 2013 who also showed an increase in dust emissions and a more realistic comparison with  
 329 satellite observations in Saudi Arabia by the introduction of an NDVI based dynamic source  
 330 mapping for GOCART model. Comparison with AERONET measurements also showed significant  
 331 improvement especially at higher AODs that are also relevant to the model efficiency for air  
 332 quality purposes (i.e. the model bias is reduced from -0.140 to 0.083 at AOD>0.25 and from -  
 333 0.933 to -0.424 at AOD>1). However, the model statistics are not improved for all AERONET  
 334 measuring stations and for all air quality states (Table2), mainly due to a possible  
 335 misclassification of dust sources in the highlands of Iran and Pakistan.

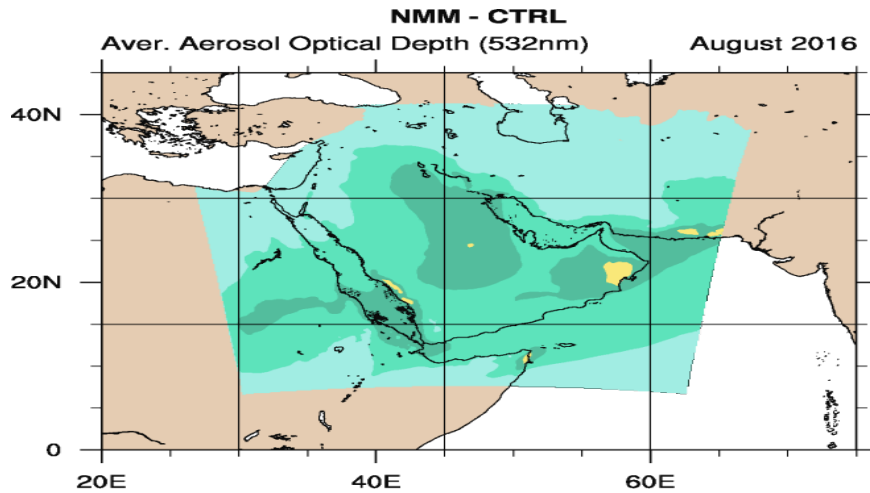
336 The main purpose of our work was the development and first testing of this new modeling  
 337 version. A major advance of our study is the ability to implement the real-time properties of

338 dust sources in air quality simulations (as represented by the satellite NDVI) and thus capture  
 339 local or seasonal effects. In general, one year is not sufficient for extracting robust statistical  
 340 results and further analysis is required to examine the performance of the proposed  
 341 methodology over longer time periods and also over different areas worldwide. For example  
 342 the simple approach of employing a uniform value of NDVI<0.1 for determining the active dust  
 343 sources may not be adequate to represent fine-scale land properties and further adjustments  
 344 may be required depending on local-scale characteristics. This new approach for the dynamic  
 345 characterization of active dust sources based on NDVI can be easily implemented in other  
 346 atmospheric dust models at different configurations and spatial coverage for improving their  
 347 performance.

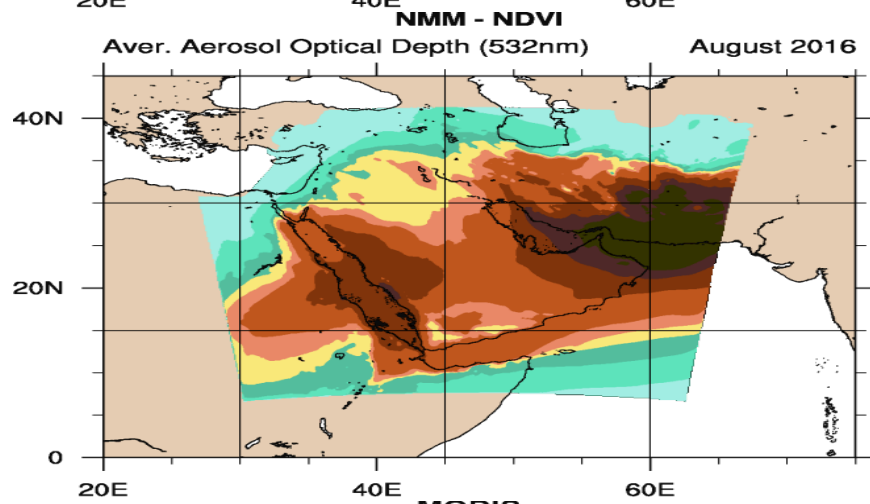
348 **Table 2. Statistical metrics at AERONET stations. Bold values indicate correlation coefficient with p <0.01.**

Station	Mean bias		RMSE		Correlation		Fractional gross error		Mean fractional bias	
	CTRL	NDVI	CTRL	NDVI	CTRL	NDVI	CTRL	NDVI	CTRL	NDVI
AgiaMarina_Xyliatou	-0.188	-0.185	0.226	0.224	-0.005	0.001	1.825	1.780	-1.828	-1.767
Cairo_EMA_2	-0.355	-0.344	0.406	0.399	<b>-0.053</b>	0.018	1.689	1.646	-1.687	-1.591
Eilat	-0.138	0.006	0.186	0.165	<b>0.110</b>	<b>0.312</b>	1.183	0.610	-1.166	0.034
El_Farafra	-0.186	-0.190	0.259	0.263	<b>0.170</b>	<b>0.138</b>	1.155	1.248	-1.218	-1.257
KAUST_Campus	-0.245	0.152	0.322	0.376	<b>0.412</b>	<b>0.386</b>	0.966	0.609	-1.001	0.342
Kuwait_University	-0.097	0.007	0.275	0.278	<b>0.152</b>	<b>0.266</b>	0.588	0.537	-0.290	0.018
Mezaira	-0.130	0.161	0.228	0.347	<b>0.353</b>	<b>0.445</b>	0.528	0.475	-0.382	0.332
SEDE_BOKER	-0.151	-0.125	0.198	0.201	0.030	0.034	1.202	1.209	-1.228	-0.921
Weizmann_Institute	-0.207	-0.180	0.264	0.255	<b>-0.088</b>	<b>-0.100</b>	1.494	1.323	-1.521	-1.197

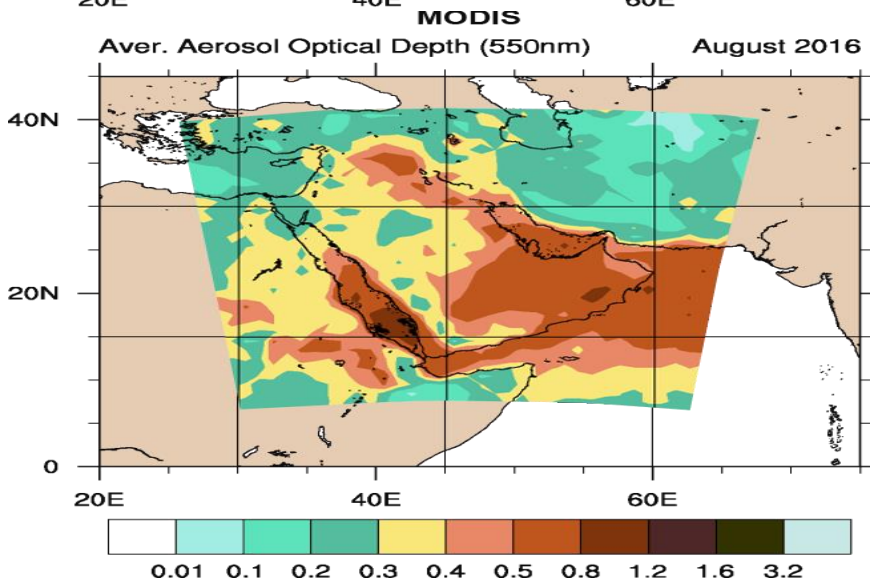
349



350



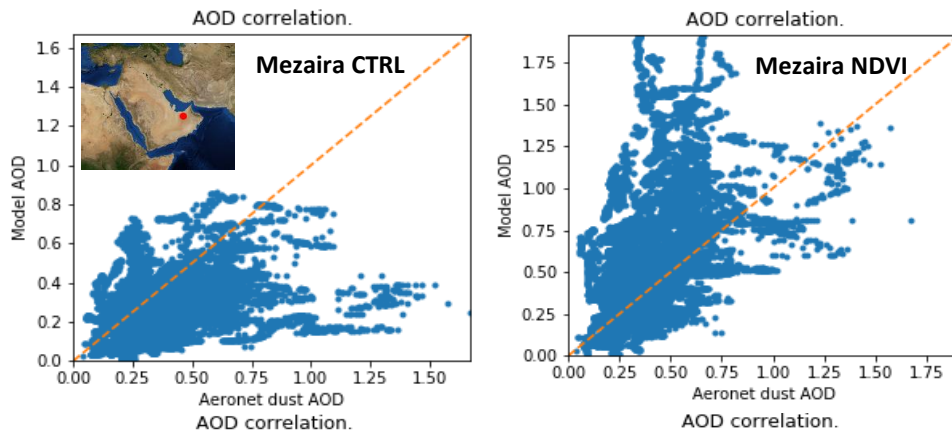
351



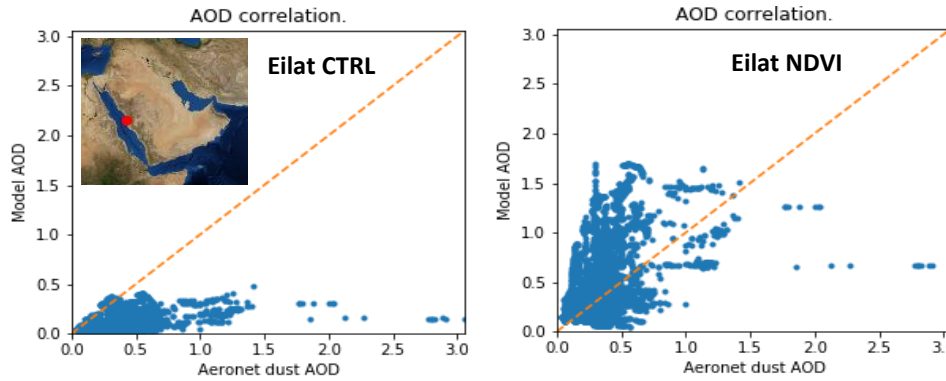
352

353 Figure 4. Monthly average simulated AOD during August 2016 from DREAM-CTRL run (a),  
 354 DREAM-NDVI run (b) and (c) MODIS. The dashed trapezoid in (c) denotes the location of the  
 355 modeling domain.

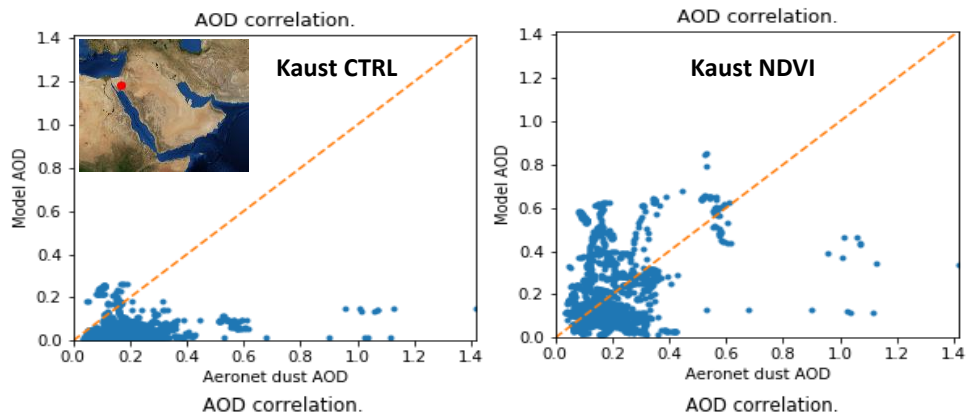
356



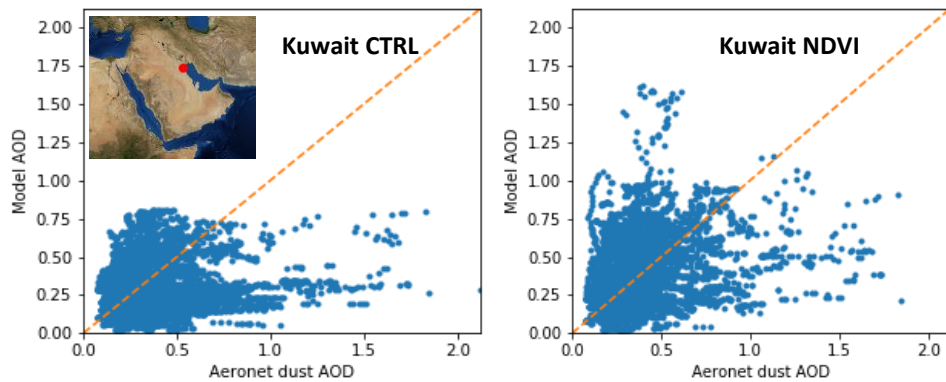
357



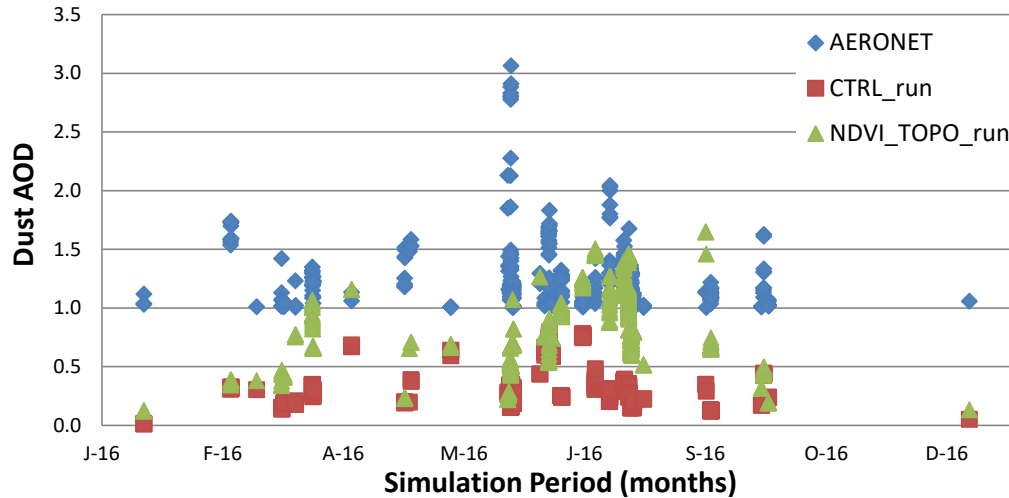
358



359



360 Figure 5. Correlation plots of modeled and AERONET dust AOD at the stations of Mezaira, Eilat,  
361 Kaust and Kuwait for 2016.



362

363 Figure 6. Timeseries of measured and modeled dust AOD for the cases of AERONET AOD>1

364

365 **Code and Data availability**

366 All code and data used in this study are available upon request.

367 **Author Contribution**

368 SS: Conceptualization, Formal analysis, Investigation, Methodology, Project administration,  
 369 Resources, Software, Validation, Visualization, Writing - original draft, Writing – review &  
 370 editing;

371 AA: Conceptualization, Funding acquisition, Project administration, Supervision, Writing –  
 372 review & editing;

373 CS: Software, Data curation, Visualization, Writing – review & editing;

374 IB: Conceptualization, Formal analysis, Software, Writing – review & editing;

375 SN: Methodology, Supervision, Writing – review & editing;

376 **Acknowledgements**

377 This work was funded by a grant from the National Space Science and Technology Center of the  
 378 United Arab Emirates University under grant number NSS Center 7 -2017. The authors also  
 379 acknowledge support from BEYOND Centre of Excellence (FP7-REGPOT-2012-2013-1,grant  
 380 agreement no. 316210) for providing financial support and computing resources.

381

382 **References**

- 383 Almazrouia, M., M. Nazrullslama, P.D. Jonesa, H. Athara and M. AshfaqrRahmana: Recent  
384 climate change in the Arabian Peninsula: Seasonal rainfall and temperature climatology of Saudi  
385 Arabia for 1979–2009. *Atmospheric Research*, 111, July 2012, p.p. 29–45., 2012
- 386 Anderson, J., E. Hardy, J. Roach, and R. Witmer: A land use and land cover classification  
387 system for use with remote sensing data, U.S. Geol. Prof. Pap. 964, U.S. Gov. Print.Off.,  
388 Washington, D. C., 1976
- 389 Anisimov, A., Tao, W., Stenchikov, G., Kalenderski, S., Prakash, P. J., Yang, Z.-L., and Shi, M.:  
390 Quantifying local-scale dust emission from the Arabian Red Sea coastal plain, *Atmos. Chem.*  
391 *Phys.*, 17, 993-1015, <https://doi.org/10.5194/acp-17-993-2017>, 2017
- 392 Arindam, C., Ravi, S., Nanjundiah and J.: Srinivasan, Impact of African orography and the  
393 Indian summer monsoon on the low-level Somali jet, *Int. J. Climatol.* 29: 983–992 (2009), DOI:  
394 10.1002/joc.1720, 2009
- 395 Boylan, J. W. and Russell, A. G.: PM and light extinction model performance metrics, goals,  
396 and criteria for three-dimensional air quality models, *Atmos. Environ.*, 40(26), 4946–4959,  
397 doi:10.1016/j.atmosenv.2005.09.087, 2006.
- 398 Brown, M. E., J. E. Pinzon, K. Didan, J. T. Morisette, and C. J. Tucker (2006), Evaluation of the  
399 consistency of long-term NDVI time series derived from AVHRR, SPOT-Vegetation, SeaWIFS,  
400 MODIS and Land-SAT ETM+, *IEEE Trans. Geosci. Remote Sens.*, 44, 1787–1793.
- 401 Chang, J. C. and Hanna, S. R.: Air quality model performance evaluation, *Meteorol Atmos*  
402 *Phys*, 87(1–3), 167–196, doi:10.1007/s00703-003-0070-7, 2004.
- 403 DeFries, R. S., and Townshend, J. R. G.: NDVI-derived land cover classifications at a global  
404 scale, *Int. J. Remote Sens.*, 15, 3567–3586, doi:10.1080/01431169408954345, 1994.
- 405 Didan, K. : MOD13A1 MODIS/Terra Vegetation Indices 16-Day L3 Global 500m SIN Grid V006  
406 [Data set].NASA EOSDIS LP DAAC.doi: 10.5067/MODIS/MOD13A1.006, 2015
- 407 Didan, K.; Munoz, A.B.; Solano, R.; Huete, A. MODIS Vegetation Index User’s Guide (MOD13  
408 Series); Version3.0; University of Arizona: Tucson, AZ, USA, 2015.
- 409 Esmail N., M. Gharagozloo, A. Rezaei, G. Grunig:. Dust events, pulmonary diseases and  
410 immune system, *Am J ClinExplmmunol* 2014 3(1):20-29, 2014.
- 411 Georgi, F. A particle dry-deposition parameterization scheme for in tracer transport models,  
412 *Journal of Geophysical Research*, 91, 9794 – 9806, 1986
- 413 Ginoux, P., Chin, M., Tegen, I., Prospero, J. M., Holben, B., Dubovik, O., & Lin, S.-J.: Sources  
414 and distributions of dust aerosols simulated with the GOCART model. *Journal of Geophysical*  
415 *Research*, 106(D17), 20,255–20,273. <https://doi.org/10.1029/2000JD000053>, 2001
- 416 Ginoux, P., J. M. Prospero, T. E. Gill, N. C. Hsu, and M. Zhao (2012), Global-scale attribution of  
417 anthropogenic and natural dust sources and their emission rates based on MODIS Deep Blue  
418 aerosol products, *Rev. Geophys.*, 50, RG3005 doi:10.1029/2012RG000388.
- 419 Holben, B.N., Eck, T.F., Slutsker, I., Tanre, D., Buis, J.P., Setzer, A., Vermote, E., Reagan, J.A.,  
420 Kaufman, Y., Nakajima, T., Lavenu, F., Jankowiak, I., Smirnov, A.: AERONET a federated  
421 instrument network and data archive for aerosol characterization. *Rem. Sens. Environ.* 66,  
422 1e16., 1998

423 Huete, A. R., Justice, C., and van Leeuwen, W., MODIS Vegetation index (MOD 13): Algorithm  
424 Theoretical Basis Document, NASA Goddard Space Flight Center, Greenbelt, Maryland 20771,  
425 1999

426 Huete, A., Didan, K., Miura, T., Rodriguez, E. P., Gao, X., & Ferreira, L. G.: Overview of the  
427 radiometric and biophysical performance of the MODIS vegetation indices. *Remote Sensing of*  
428 *Environment*, 83, 195–213., 2002

429 Janjic, Z.I., Gerrity J.P.Jr., and *Nickovic, S.*: An Alternative Approach to Nonhydrostatic  
430 Modeling. *Monthly Weather Review*, 129: 1164-1178., 2001

431 Kim, D., M. Chin, H. Bian, Q. Tan, M. E. Brown, T. Zheng, R. You, T. Diehl, P. Ginoux, and T.  
432 Kucsera: The effect of the dynamic surface bareness on dust source function, emission, and  
433 distribution, *J. Geophys. Res. Atmos.*, 118, 871–886, doi: 10.1029/2012JD017907., 2013

434 Kumar, P., Sokolik, I. N., and Nenes, A.: Measurements of cloud condensation nuclei activity  
435 and droplet activation kinetics of fresh unprocessed regional dust samples and minerals,  
436 *Atmos. Chem. Phys.*, 11, 3527–3541, doi:10.5194/acp-11-3527-2011, 2011.

437 Mahowald, N, Albani, S., Kok, J. F., Engelstaeder, S., Scanza, R., Ward, D.S., Flanner, M.G.:The  
438 size distribution of desert dust aerosols and its impact on the Earth system, *Aeolian Research*,  
439 15, 2014, Pages 53-71, <https://doi.org/10.1016/j.aeolia.2013.09.002.>, 2014

456 Mamouri, R.-E., Ansmann, A., Nisantzi, A., Solomos, S., Kallos, G., and Hadjimitsis, D. G.:  
457 Extreme dust storm over the eastern Mediterranean in September 2015: satellite, lidar, and  
458 surface observations in the Cyprus region, *Atmos. Chem. Phys.*, 16, 13711-13724,  
459 <https://doi.org/10.5194/acp-16-13711-2016>, 2016

460 Mitsakou, C., Kallos, G., Papantoniou, N., Spyrou, C., Solomos, S., Astitha, M., and Housiadas,  
461 C.: Saharan dust levels in Greece and received inhalation doses, *Atmos. Chem. Phys.*, 8, 7181-  
462 7192, <https://doi.org/10.5194/acp-8-7181-2008>, 2008.

463 Nickovic, S., G. Kallos, A. Papadopoulos, and O. Kakaliagou: A model for prediction of desert  
464 dust cycle in the atmosphere, *J. Geophys. Res.*, 106(D16), 18,113–18,129, 2001

465 Nickovic, S., Cvetkovic, B., Madonna, F., Rosoldi, M., Pejanovic, G., Petkovic, S., and Nikolic,  
466 J.: Cloud ice caused by atmospheric mineral dust – Part 1: Parameterization of ice nuclei  
467 concentration in the NMME-DREAM model, *Atmos. Chem. Phys.*, 16, 11367-11378,  
468 <https://doi.org/10.5194/acp-16-11367-2016>, 2016.

469 Olson, J. S., J. A. Watts and L. J. Allison: Carbon in Live Vegetation of Major World  
470 Ecosystems, Report ORNL-5862, Oak Ridge National Laboratory, Oak Ridge, Tennessee, USA.,  
471 1983

472 Parajuli S.P., Zender C.S., Connecting geomorphology to dust emission through high-  
473 resolution mapping of global land cover and sediment supply, *Aeolian Research* 27, 47-65,  
474 doi:10.1016/j.aeolia.2017.06.002

475 Pejanovic, G., S. Nickovic, M. Vujadinovic, A. Vukovic, V. Djurdjevic, M. Dacic: Atmospheric  
476 deposition of minerals in dust over the open ocean and possible consequences on climate.  
477 WCRP OSC Climate Research in Service to Society, 24-28 October 2011, Denver, CO, USA, 2011

478 Pérez, C., S. Nickovic, J. M. Baldasano, M. Sicard, F. Rocaadenbosch, and V. E. Cachorro: A long  
479 Saharan dust event over the western Mediterranean: Lidar, Sun photometer observations, and  
480 regional dust modeling, *J. Geophys. Res.*, 111, D15214, doi:10.1029/2005JD006579., 2006



481 Platnick, S., et al., 2017. MODIS Atmosphere L3 Monthly Product. NASA MODIS Adaptive  
482 Processing System, Goddard Space Flight Center, USA:  
483 [http://dx.doi.org/10.5067/MODIS/MOD08\\_M3.061](http://dx.doi.org/10.5067/MODIS/MOD08_M3.061)

484 Prospero J. M., P. Ginoux, O. Torres, S. E. Nicholson, and T. E. Gill: Environmental  
485 characterization of global sources of atmospheric soil dust identified with the nimbus 7 total  
486 ozone mapping spectrometer (TOMS) absorbing aerosol product, *Rev. Geophys.*, 40(1), 1002,  
487 doi:10.1029/2000RG000095, 2002

488 Rouse Jr, R. H. Haas, J. A. Schell, and D. W. Deering: "Monitoring vegetation systems in the  
489 Great Plains with ERTS." In NASA. Goddard Space Flight Center 3d ERTS-1 Symp., Vol. 1, Sect. A p  
490 309-317, 1974

491 Solano, R., K. Didan, A., Jacobson and A. Huete: MODIS Vegetation Index User's Guide, ver.  
492 2.0, Vegetation Index and Phenology Lab, <http://vip.arizona.edu>, The University of Arizona.,  
493 2010

494 Solomos, S., Kallos, G., Kushta, J., Astitha, M., Tremback, C., Nenes, A., and Levin, Z.: An  
495 integrated modeling study on the effects of mineral dust and sea salt particles on clouds and  
496 precipitation, *Atmos. Chem. Phys.*, 11, 873–892, doi:10.5194/acp-11-873-2011, 2011.

497 Solomos, S., Ansmann, A., Mamouri, R.-E., Biniotoglou, I., Patlakas, P., Marinou, E., and  
498 Amiridis, V.: Remote sensing and modelling analysis of the extreme dust storm hitting the  
499 Middle East and eastern Mediterranean in September 2015, *Atmos. Chem. Phys.*, 17, 4063-  
500 4079, <https://doi.org/10.5194/acp-17-4063-2017>, 2017

501 Spyrou, C.: Direct radiative impacts of desert dust on atmospheric water content, *Aerosol*  
502 *Science and Technology*, DOI: 10.1080/02786826.2018.1449940., 2018

503 Spyrou, C., G. Kallos, C. Mitsakou, P. Athanasiadis, C. Kalogeri and M. J. Iacono, 2013:  
504 Modeling the radiative effects of desert dust on weather and regional climate. *Atmos. Chem.*  
505 *Phys.*, 13, 5489–5504, doi:10.5194/acp-13-5489-2013, 2013

506 Spyrou, C., C. Mitsakou, G. Kallos, P. Louka, and G. Vlastou: An improved limited area model  
507 for describing the dust cycle in the atmosphere, *J. Geophys. Res.*, 115, D17211,  
508 doi:10.1029/2009JD013682., 2010

509 Torge, A., Macke, A., Heinold, B. and Wauer, J.: Solar radiative transfer simulations in  
510 Saharan dust plumes: particle shapes and 3-D effect. *Tellus B*, 63: 770-780. doi:10.1111/j.1600-  
511 0889.2011.00560.x, 2011

512 Tucker, C. J., J. E. Pinzon, M. E. Brown, D. Slayback, E.W. Pak, R. Mahoney, E. Vermote, and N.  
513 El Saleous (2005), An extended AVHRR 8-km NDVI data set compatible with MODIS and SPOT  
514 vegetation NDVI data, *Int. J. Remote Sens.*, 26, 4485–4498.

515 Vukovic, A., Vujadinovic, M., Pejanovic, G., Andric, J., Kumjian, M. R., Djurdjevic, V., Dacic,  
516 M., Prasad, A. K., El-Askary, H. M., Paris, B. C., Petkovic, S., Nickovic, S., and Sprigg, W. A.:  
517 Numerical simulation of "an American haboob", *Atmos. Chem. Phys.*, 14, 3211-3230,  
518 <https://doi.org/10.5194/acp-14-3211-2014>, 2014

519 Walko RL, Band LE, Baron J, Kittel TGF, Lammers R, Lee TJ, Ojima D, Pielke RA Sr, Taylor C,  
520 Tague C, Tremback CJ, Vidale PJ, Coupled atmosphere-biophysichydrology models for  
521 environmental modeling. *J Appl Meteor* 39: 931–944, 2000

522 Xue Y., Sellers P. J., Kinter J. L., and Shukla J.: A simplified biosphere model for global climate  
523 studies *J. Clim.* 4 345–64, 1991